

the fcc sample.

The polarized transmittance of a 6  $\mu\text{m}$  thick 2D square lattice sample is shown in Fig. 3(a), which implies the confined LC is highly aligned along the substrate. The Bragg reflection corresponds to (1 1) planes. The TM reflectance of a 12  $\mu\text{m}$  thick sample as a function of applied electric field is shown in Fig 3(b). Fig. 3(c) shows the transmittance of fcc samples. Two prominent stopbands appear in the visible transmission spectrum at normal incidence, arising from the (0 0 1) and  $(\pm 1 \pm 1)$  lattice planes. The relatively small depth of these stopbands can be attributed to the limitation of index mismatch and incomplete phase separation during holographic fabrication. For normal incidence, these stopbands were extinguished if a suitable electric field strength is applied. However, when light was incident at  $\sim 19^\circ$  from the substrate normal ( $k \approx 2\pi/\lambda(0.21 \ 0 \ 0.98)$ ), a 10 nm wavelength shift of the stopband arising from the  $(\pm 1 \ 1 \ 1)$  lattice planes was observed. The electro-optic response of this situation is plotted in Fig. 3(d).

#### 4. Summary

We successfully utilized a holographic method to fabricate tunable 2D transverse and fcc lattices in LC/polymer systems. 2D square lattice PhCs shows strong polarization dependence. The stopband of fcc samples can achieve reversible 2% wavelength shift when an electric field is applied.

#### 5. Reference

- [1] K. Busch and S. John, "Liquid-crystal photonic-band-gap materials: the tunable electromagnetic vacuum," *Phys. Rev. Lett.* **83**, 967-970 (1999).
- [2] K. Yoshino, Y. Shimoda, Y. Kawagishi, K. Nakayama and M. Ozaki, "Temperature tuning of the stop band in transmission spectra of liquid-crystal infiltrated synthetic opal as tunable photonic crystal," *Appl. Phys. Lett.* **75**, 932-934 (1999).
- [3] D. Kang, J. E. MacLennan, N. A. Clark, A. A. Zakhidov and R. H. Baughman, "Electro-optic behavior of liquid-crystal-filled silica opal photonic crystals: effect of liquid-crystal alignment," *Phys. Rev. Lett.* **86**, 4052-4055 (2001).
- [4] G. Mertens, T. Röder, R. Schweins, K. Huber and H.-S. Kitzerow, "Shift of the photonic band gap in two photonic crystal/liquid crystal composites," *Appl. Phys. Lett.* **80**, 1885-1887 (2002).
- [5] P. Mach, P. Wiltzius, M. Megens, D. A. Weitz, K. Lin, T. C. Lubensky and A. G. Yodh, "Electro-optic response and switchable Bragg diffraction for liquid crystals in colloid-templated materials," *Phys. Rev. E* **65**, #031720 (2002).
- [6] S. Foteinopoulou, A. Rosenberg, M. M. Sigalas and C.M. Soukoulis, "In- and out-of-plane propagation of electromagnetic waves in low index contrast two dimensional photonic crystals," *J. Appl. Phys.* **89**, 824-830 (2001).
- [7] M. E. Zoorob, M. D. B. Charlton, G. J. Parker, J. J. Baumberg and M. C. Netti, "Complete and absolute photonic bandgaps in highly symmetric photonic quasicrystals embedded in low refractive index materials," *Mat. Sci. and Eng.* **B74**, 168-174 (2000).
- [8] M. Campbell, D. N. Sharp, M. T. Harrison, R. G. Denning and A. J. Turberfield, "Fabrication of photonic crystals for the visible spectrum by holographic lithography," *Nature* **404**, 53-56 (2000).
- [9] L. Z. Cai, X. L. Yang and Y. R. Wang, "All fourteen Bravais lattices can be formed by interference of four noncoplanar beams," *Opt. Lett.* **27**, 900-902 (2002).
- [10] V. Berger, O. Gauthier-Lafaye and E. Costard, "Photonic band gaps and holography," *J. Appl. Phys.* **82**, 60-64 (1997).
- [11] R. L. Sutherland, V. P. Tondiglia, L. V. Natarajan, T. J. Bunning and W. W. Adams, "Electrically switchable volume gratings in polymer-dispersed liquid crystals," *Appl. Phys. Lett.* **64**, 1074-1076 (1994).
- [12] K. I. Petsas, A. B. Coates and G. Grynberg, "Crystallography of optical lattices," *Phys. Rev. A* **50**, 5173-5189 (1994).

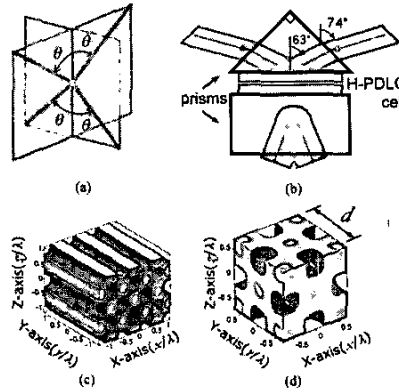


Fig. 1. Holographic formation of 2D transverse square and fcc optical lattices: (a) Ideal propagation vectors within the film, where  $\theta \approx 63^\circ$  and substrates lie in the XY-plane; (b) Opposing coupling prisms arranged to achieve required oblique propagation; (c) Calculated iso-intensity surfaces for (c) 2D transverse square lattice and (d) fcc lattice

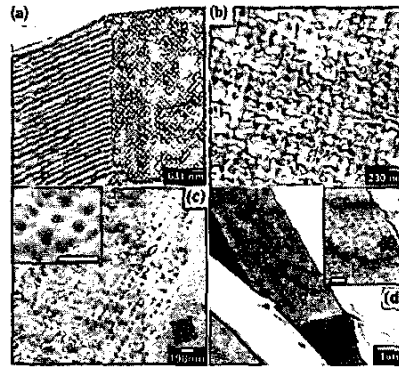


Fig. 2. Scanning electron micrographs: 2D transverse square lattice (a) and (b); fcc lattice (c) and (d).

ThJ 11:00 AM - 12:30 PM  
B206

#### System Effects of Polarization

Curtis Menyuk, UMBC, USA, Presider

ThJ1 11:00 AM

#### A Simple Formula for the Degree of Polarization Degraded by XPM and its Experimental Validation

A. Vannucci, A. Bononi, A. Orlandini, Dipartimento di Ingegneria dell'Informazione, Parma, Italy; E. Corbel, J. Thiéry, S. Lanne, S. Bigo, Alcatel Research & Innovation, Marcoussis, France, Email: vannucci@tlc.unipr.it.

We derive a closed-form expression for the DOP of polarized signals affected by XPM, in a modulated pump-probe scheme. Results are checked against simulations and experiments on a dispersion managed 3x100km link.

**Introduction:** Since the operation of many optical polarization mode dispersion (PMD) compensators (OPMDC) is based on measurement of the

degree of polarization (DOP), this study focuses on the quantification of the DOP degradation due to cross-phase modulation (XPM), which reduces the effectiveness of the OPMDC. Measurements of the system impact of DOP degradation in OPMDC are illustrated in a companion paper [1]. The nonlinear propagation of a wavelength division multiplex under the conditions of the Manakov equation [2] implies a change of the state of polarization (SOP) of each channel due to XPM, even when PMD is not present. As noted in [2], if there is significant walk-off between the channels, then such change of SOP is time-independent, and the DOP of each channel is not degraded. If walk-off is limited, however, modulation on one channel induces a time-dependent change of SOP on the others, hence a degradation of the DOP. Collings and Boivin [3] have tackled the two channels (pump and probe) case, showing that pump and probe Stokes vectors  $\mathbf{p}(z,t)$  and  $\mathbf{s}(z,t)$ , when the signals are CW, perform a rotation around a fixed pivot vector  $\mathbf{m}=\mathbf{p}(z)+\mathbf{s}(z)$  along fiber length  $z$ . Strictly speaking, when modulation is present, the pivot vector cannot be assumed constant anymore, unless the walk-off is zero.

We develop here a simplified theory in the presence of both modulation and walk-off, assuming a  $z$ -independent pivot  $\mathbf{m}(t)=\mathbf{p}(z,t)+\mathbf{s}(z,t)$  for the evaluation of the probe DOP in fibers with negligible PMD. The effect of PMD could be included in our theory as a *mixing* of the pump and probe SOPs, i.e., a randomization of their relative polarization angle: results consistent with this interpretation are reported in [1].

**Theory:** Assume that completely polarized and OOK-modulated pump and probe fields, with peak powers  $P_p$  and  $P_s$ , are launched into a fiber, with a given relative polarization angle  $\theta$  in Stokes space. According to the Manakov propagation equation [3], the local interaction of pump and probe is such that: i) if there is a "1" on both signals, they rotate around the pivot  $\mathbf{m}$ ; ii) if there is a "0" on any channel, rotation stops. Focusing on the probe Stokes vector  $\mathbf{s}(z)$  at a given position, the effect of chromatic dispersion is such that the pump *walks-off* the signal, starting and stopping the rotation of  $\mathbf{s}(z)$  around  $\mathbf{m}$ , according to its bit sequence [4]. At the fiber output  $z=L$ , the angle by which the probe has rotated around the pivot is obtained from the Manakov equation as:

$$\Psi(t) = \frac{8}{9} \gamma P_p \int_0^L e^{-\alpha z} p(t - D_c \Delta \lambda_{sp} z) dz \quad (1)$$

where  $\gamma$  is the nonlinear coefficient,  $\alpha$  the attenuation,  $D_c$  is chromatic dispersion,  $\Delta \lambda_{sp}$  is the wavelength spacing,

$$P_m = |\mathbf{m}| = \sqrt{P_p^2 + P_s^2 + 2P_p P_s \cos \theta}$$

is the peak power of the pivot, and  $p(t)$  is the normalized pump waveform modulated by the pump bit sequence.

The time-averaged value of such angle  $\langle \Psi(t) \rangle = (8/9) \gamma P_p L_{eff}/2$ , proportional to the fiber effective length, determines the average output SOP of the probe. Without loss of generality, we choose a frame of reference in which the second component of such average SOP is zero and the pivot is aligned with the third Stokes axis. Hence, we can express the time-dependent output probe SOP as,

$$\hat{\mathbf{s}}(t) = [\sin \theta, \cos \Delta \Psi(t), \sin \theta, \sin \Delta \Psi(t), \cos \theta, 1]$$

where  $\theta_0$  is the relative polarization angle between the probe and the pivot, which can be obtained from  $\theta$  and the pump-probe power ratio  $PR=P_p/P_s$  as  $\theta_0 = \theta - \arctan(\sin \theta / (PR + \cos \theta))$ . The difference rotation angle  $\Delta \Psi(t) = \Psi(t) - \langle \Psi(t) \rangle$  can be evaluated from (1) substituting  $p(t)$  with  $\Delta p(t) = p(t) - 1/2 \in [-1/2, 1/2]$ . The output probe DOP is the magnitude of the time-average of the probe SOP:

$$DOP = |\langle \hat{\mathbf{s}}(L, t) \rangle| = \sqrt{1 - \sin^2 \theta_0 \{1 - \langle \cos \Delta \Psi(t) \rangle^2 - \langle \sin \Delta \Psi(t) \rangle^2\}} \quad (2)$$

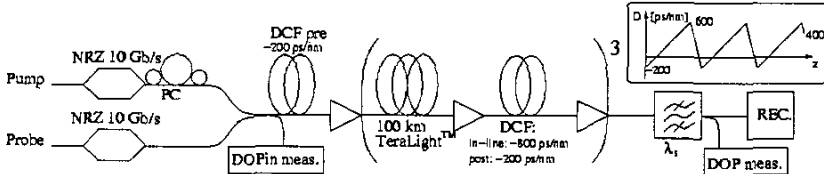


Fig. 1 Experimental set-up for total input DOP( $\theta$ ) vs output probe DOP measurements. Inset: dispersion map.

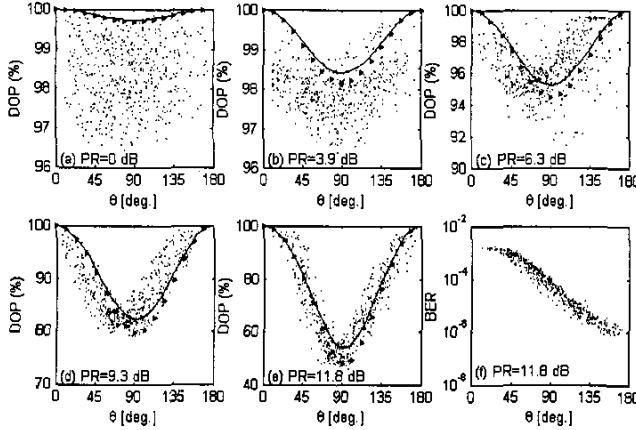


Fig. 2 (a-e) Output probe DOP after 3 spans versus relative input polarization angle  $\theta$ , for several pump-probe power ratios (PR): measurements (dots), simulations (triangles) and theory (eq. 3) (lines).

Hence, all we need is to evaluate the time-averages in (2).

Now, suppose a string of  $k$  consecutive "1" occurs in the pump bit sequence. To evaluate the effect of such string on  $\Delta\psi(t)$ , we assume to modulate the pump with a periodic sequence of  $k$  "1" followed by  $k$  "0" and so on. A periodic and skew-symmetric signal  $\Delta p(t)$  results with period  $2kT$ , being  $T$  the bit period. We can easily evaluate the angle  $\Delta\psi(t)$  from (1) if we approximate  $\Delta p(t)$  with the first harmonic of its Fourier series expansion:  $\Delta p(t) \approx (4/\pi) \sin(\omega_0 t/k)/2$ , where  $\omega_0 = \pi/T$  is the frequency of the 1010... bit sequence. Note that the integral in (1) is the convolution of the normalized pump with a walk-off filter  $H(\omega)$ , whose amplitude response can be approximated as  $|H(\omega)| \approx [\alpha^2 (\omega D_c \Delta\lambda_p)^2]^{1/2}$  for long fibers ( $L \gg 1/\alpha$ ) [5]. Hence, one gets  $\Delta\psi(t) = (8/9) \gamma P_m H(\omega_0/k) (4/\pi) \sin(\omega_0 t/k + \phi_0)/2$ . To evaluate the time-averages in (2), we can expand  $\cos\Delta\psi(t)$  and  $\sin\Delta\psi(t)$  in Fourier series. Averaging over periods much longer than  $2kT$ , one gets  $\langle \sin\Delta\psi(t) \rangle = 0$ , and  $\langle \cos\Delta\psi(t) \rangle \approx J_0(\Delta\psi_M(k))$ , where  $J_0$  is the zero-th order Bessel function of the first kind, and  $\Delta\psi_M(k) = (8/9) \gamma P_m H(\omega_0/k) (4/\pi)/2$  is the maximum swing angle for the probe SOP.

Of course, when the pump is modulated by a pseudo random bit sequence (PRBS), we should consider all possible strings of  $k$  ones ( $k=1 \dots 8$ ). In an uncoded PRBS, the relative occurrence of such strings is  $1/2^k$ . Resorting to the ergodicity of the process  $\Delta\psi(t)$ , we can evaluate the time-average  $\langle \cos\Delta\psi(t) \rangle$  through the summation of  $J_0(\Delta\psi_M(k))$  terms weighted by their relative occurrence. Propagation on more than one span can be easily accounted for by multiplying the arguments of the  $J_0$  functions by  $N_{\text{spans}}$ , provided that fiber losses are recovered and in-line dispersion is perfectly compensated at each span. The final formula for the DOP is:

$$DOP = \sqrt{1 - \sin^2 \theta} \left[ 1 - \sum_{k=1}^8 \frac{1}{2^k} J_0 \left( \frac{(8/9) \gamma P_m (2/\pi) N_{\text{spans}}}{\sqrt{\alpha^2 + (\pi D_c \Delta\lambda_p / (kT))^2}} \right) \right] \quad (3)$$

which is an approximation, since we are only approximating an actual PRBS. The dependence of the DOP on the relative pump-probe polarization angle  $\theta$  can be made explicit by using the two relations given above for  $\theta_s$  and  $P_m$ . From (3), we

see that, if polarization control of the signals ( $\theta=180^\circ$  or  $\theta=0^\circ$ ) cannot be achieved, e.g., due to PMD, the basic countermeasure against DOP degradation is to increase the walk-off by further spacing the channels or by using a more dispersive fiber. Increasing the bit rate implies both a smaller  $T$  and a larger  $\Delta\lambda_p$  in (3), hence a reduction of XPM-induced DOP degradation.

**Experimental and simulations results:** We performed DOP measurements on the dispersion-managed 3x100 km link depicted in Fig. 1. The dispersion map is shown in the inset. We used TeraLight<sup>TM</sup> as the transmission fiber, with  $\alpha=0.2$  dB/km,  $\gamma=1.68$  W<sup>-1</sup>km<sup>-1</sup> and  $D_c=8$  ps/nm/km, whose total measured DGD on the link is below 2 ps, so that PMD can be safely neglected. Pump and probe are spaced by  $\Delta\lambda_p=0.8$  nm and are NRZ modulated at 10 Gb/s by independent bit sequences.

We performed five sets of 500 measurements of both the total input DOP and the output DOP, after filtering the probe channel, randomly changing the polarization controller (PC) each time. Fig. 2a-e reports the measured probe DOP (dots) versus  $\theta$ , along with simulation results (triangles), and the theoretical DOP curve (3) (solid line). The average probe power is fixed at 3 dBm ( $P_s=6$  dBm) while the power ratio PR is varied for each set of measurements. The relative polarization angle  $\theta$  can be easily calculated from the measured input DOP and the power ratio PR.

Fig. 2f reports BER measurements for the same case of Fig. 2e. Without giving details about the receiver, the purpose of this figure is to show that, as  $\theta$  increases, the efficiency of XPM is reduced by the misalignment of pump and probe polarizations and, as is well known, the best performance is obtained for orthogonally polarized (in Jones space) channels ( $\theta=180^\circ$ ).

All plots in Fig. 2(a-e) have the same V-shape. Their symmetry, however, is related to our system parameters and is not a general feature of (3). In fact, by increasing  $P_s$ , a shift of the minimum towards larger  $\theta$  values is observed from (3). We use different DOP scales to highlight the cases in which the pump power is smaller. The spread in the measurement points is mainly due to the amplifiers noise, which is the main source of depolarization when XPM is negligible (small PR). Such effect is not taken into account in the-

ory and simulations. A very good fit is observed, hence eq. (3) allows an easy closed-form prediction of system behavior with good accuracy.

**Conclusions:** We derived a closed-form approximate expression for the DOP of a signal degraded by the XPM of a nonlinearly interfering pump. Although in the absence of PMD, DOP degradation does not affect the BER, the quantification of this effect is useful to assess the performance of OPMDCs driven by the DOP as a feedback signal. Experimental measurements, as well as simulations, confirm the good accuracy of the derived expression.

#### References

- [1] E. Corbel, J.-P. Thiéry, S. Lanne, S. Bigo, A. Vannucci and A. Bononi, "Experimental statistical assessment of XPM impact on optical PMD compensator efficiency," *submitted to OFC 2003*.
- [2] D. Wang and C. R. Menyuk, "Polarization Evolution Due to the Kerr Nonlinearity and Chromatic Dispersion," *IEEE J. Lightwave Technol.*, 17, 2520-2529 (1999).
- [3] B. C. Collings and L. Boivin, "Nonlinear Polarization Evolution Induced by Cross-Phase Modulation and Its Impact on Transmission Systems," *IEEE Photon. Technol. Lett.* 12, 1582-1584 (2000).
- [4] Z. Pan, Q. Yu, A. E. Willner, and Y. Arieli, "Fast XPM-induced polarization-state fluctuations in WDM systems and their mitigation," in *Proc. OFC 2002*, paper ThA7, 379-381 (2002).
- [5] A. Bononi, C. Francia, and G. Bellotti, "Impulse Response of Cross-Phase Modulation Filters in Multi-span Transmission Systems with Dispersion Compensation," *Optical Fiber Technology* 4, 371-383 (1998).

ThJ2

11:15 AM

#### Experimental Statistical Assessment of XPM Impact on Optical PMD Compensator Efficiency

E. Corbel, J. P. Thiéry, S. Lanne, S. Bigo, Alcatel Research & Innovation, Marcoussis, France; A. Vannucci, A. Bononi, Università di Parma, Parma, Italy, Email: Erwan.Corbel@alcatel.fr

In this paper, we report experiments on the statistical assessment of the reduction of PMD mitigator efficiency in presence of XPM effects. The XPM-induced depolarization limits compensation in polarization dispersive ultra-long haul system at 10 Gb/s.

#### 1. Introduction

Since Polarization-Mode Dispersion (PMD) has been designated as a major impairment for optical transmission systems, many types of optical PMD compensator (OPMDC) have been proposed, starting from the simple mitigator [1] and heading for mitigation of higher-order components of PMD [2].

The system generally corresponds to a non-realistic transmission because it consists of an (higher-order) emulator followed by the compensator. In other words, other propagation effects such as Chromatic Dispersion (CD) and Kerr effects are not often taken into account, for computation time reasons, even if some papers focused on chirp effects on compensation [3] or studied the behavior of Degree of Polarization (DOP) as feedback signal in presence of Self-Phase Modulation (SPM) [4]. That lack is all the more important that we are already aware of the subtle interplay between Kerr non-linearities, chromatic dispersion and PMD [5].

In the same context, some have recently shown that XPM effects make the PMD mitigator be less efficient [6,7]. The purpose of this paper is to experimentally check the reduction of PMD mitigation efficiency from a statistical point of view.

#### 2. Considerations about XPM impact on PMD compensation

In this paper we focus on first-order compensation. It consists of a polarization controller and a piece of Polarization Maintaining Fiber (PMF) (see OPMDC on figure 1-a). The mitigator aims at inverting PMD conditions that the incoming